

REPORT DOCUMENTATION PAGE			<i>Form Approved</i> <i>OMB No. 0704-0188</i>	
Public reporting burden for this collection of information is estimated to average 1 hour per response, including the time for reviewing instructions, searching existing data sources, gathering and maintaining the data needed, and completing and reviewing this collection of information. Send comments regarding this burden estimate or any other aspect of this collection of information, including suggestions for reducing this burden to Department of Defense, Washington Headquarters Services, Directorate for Information Operations and Reports (0704-0188), 1215 Jefferson Davis Highway, Suite 1204, Arlington, VA 22202-4302. Respondents should be aware that notwithstanding any other provision of law, no person shall be subject to any penalty for failing to comply with a collection of information if it does not display a currently valid OMB control number. PLEASE DO NOT RETURN YOUR FORM TO THE ABOVE ADDRESS.				
1. REPORT DATE (DD-MM-YYYY) 10-11-2010		2. REPORT TYPE Proceedings		3. DATES COVERED (From - To) NOV 2010 - DEC 2010
4. TITLE AND SUBTITLE Doppler-Offset Waveforms for MIMO Radar			5a. CONTRACT NUMBER FA8720-05-C-0002	
			5b. GRANT NUMBER	
			5c. PROGRAM ELEMENT NUMBER	
6. AUTHOR(S) Daniel Rabideau			5d. PROJECT NUMBER	
			5e. TASK NUMBER	
			5f. WORK UNIT NUMBER	
7. PERFORMING ORGANIZATION NAME(S) AND ADDRESS(ES) MIT Lincoln Laboratory 244 Wood Street Lexington, MA 02420			8. PERFORMING ORGANIZATION REPORT NUMBER	
9. SPONSORING / MONITORING AGENCY NAME(S) AND ADDRESS(ES) ESC/CAA 20 Schilling Circle, Bldg 1305 Hanscom AFB, MA 01731			10. SPONSOR/MONITOR'S ACRONYM(S) ESC/CAA	
			11. SPONSOR/MONITOR'S REPORT NUMBER(S)	
12. DISTRIBUTION / AVAILABILITY STATEMENT DISTRIBUTION STATEMENT A. Approved for public release; distribution is unlimited.				
13. SUPPLEMENTARY NOTES				
14. ABSTRACT In a Multiple-Input, Multiple-Output (MIMO) radar, independent waveforms are transmitted from different locations, with the resulting reflections processed to form a "virtual antenna array" that is larger than the physical aperture of the radar. This paper examines the design of Doppler-offset waveforms for use in adaptive MIMO GMTI radar systems. Such waveforms provide good adaptive cancellation performance, but are also subject to strong range and Doppler ambiguities. We analyze these ambiguities, and show how they relate to array topology and waveform design. Then, we describe a new waveform approach, called "Dithered DDMA", which enables high performance clutter cancellation over large range-Doppler regions without introducing ambiguous ranges or blind speeds, and without increasing the computational load on the MIMO processor.				
15. SUBJECT TERMS				
16. SECURITY CLASSIFICATION OF: U			17. LIMITATION OF ABSTRACT SAR	18. NUMBER OF PAGES 13
a. REPORT U	b. ABSTRACT U	c. THIS PAGE U		
				19b. TELEPHONE NUMBER (include area code) 781-981-5997

Doppler-Offset Waveforms for MIMO Radar

October 2010

Daniel J. Rabideau

MIT Lincoln Laboratory
Lexington, MA

ABSTRACT

In a Multiple-Input, Multiple-Output (MIMO) radar, independent waveforms are transmitted from different locations, with the resulting reflections processed to form a "virtual antenna array" that is larger than the physical aperture of the radar. This paper examines the design of Doppler-offset waveforms for use in adaptive MIMO GMTI radar systems. Such waveforms provide good adaptive cancellation performance, but are also subject to strong range and Doppler ambiguities. We analyze these ambiguities, and show how they relate to array topology and waveform design. Then, we describe a new waveform approach, called "Dithered DDMA", which enables high performance clutter cancellation over large range-Doppler regions without introducing ambiguous ranges or blind speeds, and without increasing the computational load on the MIMO processor.

Previously released material.
ESC clearance number provided.

ESC-10-0963 8D 11/10/10

This work was sponsored by the United States Air Force under Air Force Contract FA8721-05-C-0002. Opinions, interpretations, conclusions, and recommendations are those of the authors and are not necessarily endorsed by the United States Government.

1.0 Introduction

Multiple-Input, Multiple-Output (MIMO) radar concepts have recently been proposed for both airborne and surface-based radar applications [1-13]. In a MIMO radar, N_t transmit antennas each emit a unique waveform. These waveforms propagate through the environment, where they are reflected by targets and other objects, and subsequently received by N_r receive antennas. Each receiver is connected to a bank of filters, with one filter tuned to each of the transmitted waveforms. Collectively, these filter outputs form $N_t \cdot N_r$ data channels that can then be combined as desired, e.g., to maximize Signal to Interference plus Noise Ratio (SINR).

In the literature, MIMO radars have been shown to provide a number of potential benefits as compared with normal phased-array radars (i.e., radars that emit a single coherent transmit beam that is later received using [1] an array of receive antennas). These benefits include: increased angle resolution [1-6], increased Doppler resolution [1, 7], reduced clutter levels (and related hardware requirements) [1], sharper airborne radar clutter notches [2, 7, 13], and Lower Probability of Intercept [1].

To achieve these benefits, most of the literature has assumed the use of “orthogonal” waveforms. In practice, however, such waveforms do not exist and must be approximated. This, in turn, has prompted research into the area of waveform design [14-16], with such research producing a variety of frequency offset waveform concepts. Among these, Doppler Division Multiple Access (DDMA), in which waveforms are offset in frequency within the Doppler band of the radar, offers particular promise.

After describing the MIMO radar signal environment (Section 2.0), we briefly review the theory underlying Doppler-offset waveforms (Section 3.0). In particular, we describe how DDMA waveforms achieve “quasi-orthogonality” by exploiting prior knowledge of the signal environment. Then, in Section 3.1, we discuss the range and Doppler ambiguities associated with DDMA waveforms. In Section 3.2, these ambiguities are shown to lead to “phantom blind speeds” and other problems. Section 3.3 analyzes these ambiguities, and shows how they are related to array topology and waveform parameters. Then, in Section 4.0, we describe a modified DDMA waveform approach that enhances both target detection and clutter cancellation in airborne MTI systems and related radar applications.

2.0 MIMO Radar Principles

Consider an array of N_t transmit antennas and N_r receive antennas. In MIMO radar, each transmit antenna radiates an independent waveform \mathbf{s}_n . Here, \mathbf{s}_n denotes an $L \times 1$ vector containing complex baseband samples of the n^{th} transmit waveform. Collectively, these N_t transmit waveforms form an $N_t \times L$ signal matrix, $\mathbf{S} = [\mathbf{s}_1 \ \mathbf{s}_2 \ \dots \ \mathbf{s}_{N_t}]^T$. These N_t waveforms propagate through the environment, where they are reflected by both targets and clutter. In particular, the waveforms reflected from point-target t will create a signal that is proportional to $\mathbf{a}_{Tx}^T(\Theta_t)\mathbf{S}$, where $\mathbf{a}_{Tx}(\Theta_t)$ denotes the $N_t \times 1$ response vector for the transmit array. Here, Θ_t represents a set of target signal parameters describing the target t . In typical airborne radar systems, for example, $\Theta_t = \{\theta_t, \zeta_t\}$ where θ_t and ζ_t are the azimuth and depression angles from the radar to target t , respectively.

The reflected signal then propagates through the environment and is received by an array of antennas. Assuming each receiver collects $R \gg L$ samples, the $N_r \times R$ sample matrix at the output of the receive array has the form

$$\mathbf{X} = \sum_t \alpha(\Theta_t) \mathbf{a}_{Rx}(\Theta_t) \mathbf{a}_{Tx}^T(\Theta_t) \mathbf{S}_t + \sum_c \alpha(\Theta_c) \mathbf{a}_{Rx}(\Theta_c) \mathbf{a}_{Tx}^T(\Theta_c) \mathbf{S}_c + \mathbf{N} \quad (1)$$

where subscripts t and c index into the set of targets and clutter patches, respectively. Here, $\alpha(\Theta_t)$ represents a complex scale factor associated with target t , while $\mathbf{a}_{Rx}(\Theta_t)$ denotes the receive array's $N_r \times 1$ response vector for target t . The $N_r \times R$ matrix \mathbf{S}_t , on the other hand, describes how the various

waveforms propagate to, and are reflected by, target t . That is, the n^{th} column of \mathbf{S}_t contains the convolution of \mathbf{s}_n with the target's impulse response. Furthermore, since $R \gg L$, \mathbf{S}_t will also contain many zeros to account for propagation delays to/from the target. Variables $\alpha(\Theta_c)$, $\mathbf{a}_{Rt}(\Theta_c)$, $\mathbf{a}_{Tx}(\Theta_c)$ and \mathbf{S}_c are defined similarly with respect to the c^{th} clutter patch. Lastly, the $N_r \times R$ matrix \mathbf{N} represents noise as well as other interference.

After being received, the sample matrix is processed to extract target detections and/or to form images. Target detection, for example, can be performed by passing the received samples through a bank of matched filters. Often, this filtering is implemented in stages, wherein the initial stage applies a set of "waveform" matched filters to form $N_t \times R'$ matrices,

$$\mathbf{Y}_m = \begin{bmatrix} \mathbf{x}_m^T * \mathbf{h}_1^T \\ \vdots \\ \mathbf{x}_m^T * \mathbf{h}_N^T \end{bmatrix}, \quad m=1, \dots, N_r \quad (2)$$

where \mathbf{x}_m^T denotes the m^{th} row of \mathbf{X} , $*$ denotes convolution, and \mathbf{h}_n denotes the $L \times 1$ matched filter for signal \mathbf{s}_n . After matched filtering, the rows of the $N_t N_r \times R'$ matrix $\mathbf{Y} = [\mathbf{Y}_1^T \ \dots \ \mathbf{Y}_{N_r}^T]^T$ represent $N_t N_r$ channels of data. It is thus possible to coherently combine these channels,

$$\mathbf{z} = \mathbf{w}^H \mathbf{Y} \quad (3)$$

to achieve some desired goal (note: incoherent combining of channels has also been used [9, 17]; however, this approach will not be discussed further here). Often, \mathbf{w} is chosen to maximize SINR, i.e.,

$$\max_{\mathbf{w}} \frac{|\mathbf{w}^H \mathbf{v}_{tgt}|^2}{\mathbf{w}^H \mathbf{R} \mathbf{w}} \quad (4)$$

where \mathbf{v}_{tgt} is the target response vector. The solution to this problem is known to be $\mathbf{w} = \gamma \mathbf{R}^{-1} \mathbf{v}_{tgt}$, where $\mathbf{R} = E\{\mathbf{Y}_o \mathbf{Y}_o^H\} = \mathbf{R}_C + \mathbf{R}_N$, \mathbf{Y}_o are target-free snapshots formed in a manner similar to \mathbf{Y} , \mathbf{R}_C is the clutter covariance matrix, \mathbf{R}_N is a noise covariance matrix, and γ is a nonzero complex constant.

3.0 Doppler-Division Multiple Access Waveforms

Adaptive MIMO radar performance depends on the availability of "orthogonal" transmit signals. To date, much research has been conducted to identify waveform sets that are approximately orthogonal. Toward that end, one approach that is often discussed is Frequency Division Multiple Access, or FDMA.

In the MIMO radar literature, the term FDMA is used, generically, to refer to sets of waveforms occupying different frequencies at the same time. Mathematically, the n^{th} FDMA waveform can be written as:

$$s_n(t) = s(t) e^{j2\pi f_n t} \quad 0 \leq t \leq T. \quad (5)$$

for $n=1, \dots, N_t$, where $s(t)$ is a common radar waveform of bandwidth B , and f_n is the carrier frequency for waveform n . Usually, the carrier frequencies are stepped linearly, e.g.,

$$f_n = f_0 + (n-1)\Delta f \quad (6)$$

where f_0 is the base carrier, and Δf is the frequency step size. In the context of MIMO radar, such waveforms are considered quasi-orthogonal as long as:

$$s_{i,j}(t, \tau_c) \cong 0 \quad (7)$$

i.e., $s_{i,j}(t, \tau_c)$ must be negligibly small (with respect to noise) whenever $i \neq j$.

On transmit, FDMA MIMO radars emit all N_r frequency offset waveforms simultaneously. Then, each of the N_r received signals is processed via a bank of matched filters – one filter for each waveform. Each filter, in essence, demodulates a single transmit signal and compresses it in range.

There are many types of FDMA waveforms. For simplicity, we classify these into three groups (“noninterleaved,” “coarsely interleaved,” and “finely interleaved”) according to the separation between their spectral bands, as illustrated in Figure 1 (for the case of $N_r = 2$).

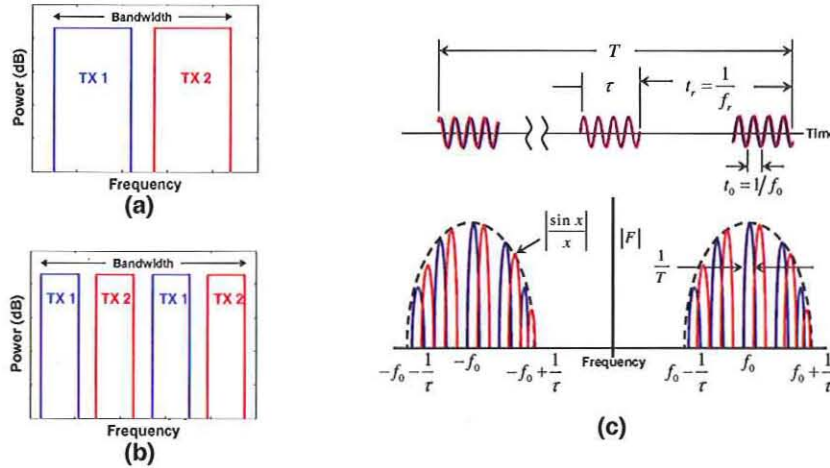


Figure 1. Examples of FDMA waveforms.
 (a) Non-interleaved waveforms, (b) Coarsely interleaved waveforms,
 (c) Finely interleaved waveforms.

Noninterleaved FDMA waveforms (see Figure 1a) employ frequency offsets that are larger than the signal bandwidth, i.e., $|\Delta f| \geq B$, to separate the transmitted waveforms during each transmit pulsewidth (i.e., $T = \tau$). Interleaved FDMA waveforms, on the other hand, employ smaller frequency offsets within an overlapping frequency band (see Figure 1b-c). In either case, frequency offsets must be large enough to isolate the Doppler bandwidth of the signals of interest – otherwise ambiguities will occur.

By design, all three of these basic FDMA waveform types are “orthogonal” in the sense of (7). Unfortunately, a MISO Cancellation Ratio (MCR) analysis [18] reveals a significant limitation for FDMA. In particular, the adaptive cancellation performance, as measured by MCR, degrades quickly as the frequency offset grows, according to:

$$MCR \cong 1 - \left(\frac{\sin(\pi \Delta f / B)}{\pi \Delta f / B} \right)^2. \quad (8)$$

In fact, it is clear from (8) that the only way to achieve good MCR is to interleave the FDMA waveform bands, with fine interleaving preferred over coarse interleaving.

One approach toward such fine interleaving is to use

$$\Delta f \leq f_r / N_r, \quad (9)$$

Then, each of the N_r transmit waveforms will occupy a “slice” of the radar’s unambiguous Doppler band, as shown in Figure 1c. On receive, the MIMO processor can then use conventional Dopplers filters to isolate each transmit channel. Such waveforms are called Doppler Division Multiple Access (DDMA).

In practice, the phase modulation defined by (5)-(6) and (9) is approximately constant over short time intervals such as the radar pulsewidth τ . Hence, the DDMA frequency modulation can be approximated via a piecewise constant phase modulation. That is, the n^{th} frequency shifted waveform is created by applying a phase modulation to the common waveform

$$s_n(t) = s(t)e^{ju_n(p)} \approx s(t)e^{j2\pi f_n t} \quad 0 \leq t \leq T \quad (10)$$

where $u_n(p) = 2\pi f_n p / f_r$ denotes the phase value applied to transmitter n during PRI $p = \lfloor f_r t \rfloor$. This approximation enables simplified array hardware, since each transmit channel requires only a phase shifters (rather than a means of independently generating frequency offset waveforms). More importantly, by the analysis of [18], excellent clutter cancellation can be achieved.

In the discussion that follows, we focus on DDMA waveforms as defined by (6) and (9) – (10). However, many of the issues we describe will apply to systems employing true (i.e., continuously modulated) DDMA as well.

3.1. DDMA Ambiguities

To receive signals (including both targets and clutter) unambiguously, the DDMA PRF must satisfy

$$f_r / N_t \geq \Delta f \geq B_D. \quad (11)$$

For large N_t and B_D , such DDMA waveforms will have relatively high PRFs. In Ground Moving Target Indication (GMTI) radar, for example, these PRFs ($f_r \geq N_t B_D$) will be up to N_t times higher than “normal” SIMO GMTI radar PRFs ($f_r \geq B_D$). As a result, there can be a larger number of both “range ambiguities” and range eclipsed regions[†].

To address the problem, we could lower the PRF to:

$$f_r / N_t \geq \Delta f \geq B_C \quad (12)$$

(where B_C is the Doppler bandwidth associated with clutter), resulting in PRFs that (1) are high enough so as to unambiguously isolate the clutter from each transmit/receive signal path, but (2) allow high speed targets to become Doppler ambiguous. In this case, a high speed target signal received via one transmit/receive signal path will look the same as a low speed target signal (or clutter signal) received via a different transmit/receive signal path. When this happens, high speed targets will “fold over” onto low speed targets. Moreover, some high speed targets will alias into the blind zones associated with the low-speed clutter.

Lowering the PRF further, to $f_r / N_t \geq \Delta f \geq \epsilon B_C$ with $\epsilon < 1$, leads to additional problems. Such low PRFs increase the clutter rank and require additional degrees of freedom for clutter suppression. Hence, most systems will choose to operate in the PRF regime dictated by (12) – which results in Doppler ambiguous high speed targets.

3.2. Impact of Ambiguities

The performance of DDMA using (12) is illustrated in a. Here, a sidelooking airborne GMTI radar is simulated. The radar uses $N_t = 16$ transmit elements, arranged linearly with an inter-element spacing of $d_E = 0.19$ m, and $N_r = 1$ receiver element. The element gain is 13 dBi and the wavelength is $\lambda = 0.1265$ m. The radar platform is moving at $v = 27.5$ m/s at an altitude of 10000 ft.

[†] Range ambiguities and eclipsing could be reduced by re-designing the radar to smaller N_t or B_D . For the remainder of this paper, however, N_t and B_D are assumed fixed.

According to the theory of airborne adaptive radar [19], this radar's mainlobe clutter should have a Doppler spread of $\pm 2\nu\cos(\zeta_D)\sin(\theta_B)/\lambda$. In our simulation, the ground was illuminated at a slant range of 6 km (corresponding to a depression angle of $\zeta_D = 30^\circ$) and, due to element pattern effects, the radar's mainlobe clutter power fell below noise at an azimuth offset of $\theta_B \cong 34^\circ$. Consequently, the Doppler spread is $\pm 2\nu\cos(\zeta_D)\sin(\theta_B)/\lambda \cong \pm 210.5$ Hz, corresponding to a Doppler bandwidth of $B_C = 421$ Hz. Had our system used a single transmit phase center (i.e., SIMO radar with $N_t = 1$), all this clutter would appear in a single Doppler band (spread over ± 210.5 Hz). With $N_t = 16$ transmitters, however, the clutter spectrum contains multiple clutter bands, as shown in a. In the MIMO case, each of these $N_t - 1$ "extra" clutter bands is associated with one of our $N_t - 1$ Doppler-offset transmit waveforms. In particular, the n^{th} transmitter's clutter is shifted by $(n-1)\Delta f$ Hz. In our simulation, we used a PRF of $f_r = 6745$ Hz and a frequency offset of $\Delta f = f_r/N_t = 421.6$ Hz, yielding a shift of $(n-1)\Delta f = 421.6n - 421.6$ Hz. This relationship (i.e., the mapping of transmitters to clutter bands) is made explicit via the annotations at the top of a.

For GMTI radar, the multi-band clutter spectrum (depicted in a) must be cancelled to detect moving targets. Fortunately, since our frequency offset ($\Delta f = 421.6$ Hz) is larger than the total clutter bandwidth ($B_C = 421$ Hz), the clutter return from each transmitter is well-isolated in the Doppler domain. This isolation allows the MIMO signal processor to unambiguously isolate the clutter due to each transmit phase center. The MIMO receiver can then use these degrees of freedom to cancel the clutter.

Fast targets, however, will remain Doppler ambiguous and will thus alias back into the endo-clutter region. b – c depicts the resulting SINR losses after adaptive clutter cancellation[‡]. Note that the maximum possible clutter Doppler shift, $2\nu\cos(\zeta_D)\sin(\theta_B)/\lambda \cong 210.5$ Hz, occurs when clutter is received from the leading edge of the element pattern. Likewise, the minimum Doppler shift, $-2\nu\cos(\zeta_D)\sin(\theta_B)/\lambda \cong -210.5$ Hz, occurs when clutter is received from the aft edge of the element pattern. At all other angles in between, the clutter Doppler varies according to

$$2\nu\cos(\zeta_c)\sin(\theta_c)/\lambda, \quad (13)$$

forming a "ridge" when viewed in the Doppler-spatial frequency plane. Now, had our system used just a single transmit phase center ($N_t = 1$), (13) dictates the existence of a single clutter ridge. SINR losses would be high along this ridge, but close to zero elsewhere. With $N_t = 16$ Doppler-offset transmit waveforms, however, the aggregate frequency shift associated with transmitter n and clutter patch c will be

$$(n-1)\Delta f + 2\nu\cos(\zeta_c)\sin(\theta_c)/\lambda. \quad (14)$$

Consequently, there will be N_t clutter ridges. This results in $N_t - 1$ additional ridges of high SINR loss, as shown in b[§]. This also means there will be $N_t - 1$ new "blind speeds" caused by the DDMA waveform at any given target angle. c shows a cut through the SINR loss plot at array broadside. There, we see N_t narrow Doppler regions (i.e. target speeds) having high loss due to the clutter nulls formed during STAP processing. Comparable low-PRF SIMO radars, in contrast, would have only a single blind speed.

[‡] To make these plots, the $N_t N_r$ MIMO channels were adaptively weighted and combined using Space-Time Adaptive Processing (STAP). STAP is a variation on the SINR maximization process of (3) – (4) used to adaptively cancel clutter [WARD]. In a STAP system, adaptive clutter nulls are automatically adjusted, as a function of Doppler, to track clutter. Losses will occur in regions that are close to the clutter manifold. These "SINR Losses," which are depicted in b – c, are computed as the ratio of the STAP processed output to the ideal, nonadaptively processed output in an interference free environment. Hence, a loss of 0 dB is ideal, while large negative values indicate regions of high loss.

[§] Note that b plots loss as a function of Doppler frequency and normalized spatial frequency, with normalized spatial frequency defined as $d_E \cos(\zeta_i)\sin(\theta_i)/\lambda$.

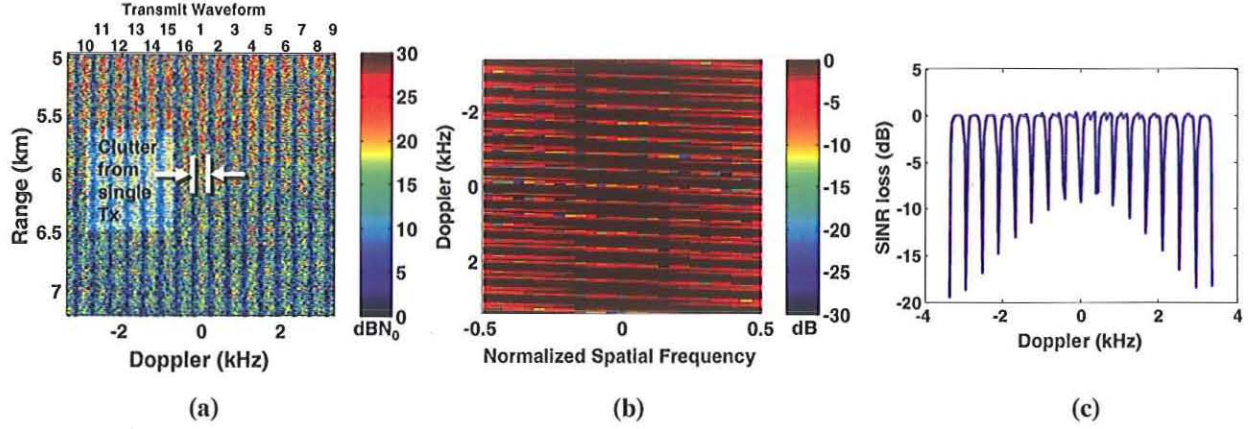


Figure 2. GMTI radar using DDMA waveform ($N_t = 16$, $N_r = 1$).
(a) Clutter spectrum, (b) SINR Loss after STAP processing (we used the PRI-staggered post-Doppler STAP algorithm of [19]), (c) SINR loss at broadside

3.3. Analysis of Ambiguities

The $N_t - 1$ extra clutter ridges, discussed in Section 3.2, occur because fast targets (i.e., any target t having Doppler shift $d_t \in D^{FAST} \equiv \{d_t : |d_t| > f_r/2N_t\}$) alias in Doppler. In some cases, the aliased Doppler will be on (or near) the clutter ridge. When this happens, the STAP weights used to receive a target t (as defined by parameters $\Theta_t = \{\theta_t, \zeta_t, d_t \in D^{FAST}, z_t\}$) are nearly the same as the weights used to receive a slow target t' (as defined by $\Theta_{t'} = \{\theta_{t'}, \zeta_{t'}, d_{t'}, z_{t'}\}$ where $d_{t'} \in D^{SLOW} \equiv \{d_{t'} : |d_{t'}| \leq f_r/2N_t\}$) – resulting in a loss when the later is close to the true clutter ridge (aka blind speed).

In SIMO radar, this sort of aliasing occurs when the target Doppler is $|d_t| > f_r/2$. Such targets are called “Doppler ambiguous”. In DDMA MIMO radar, Doppler aliasing occurs at slower target speeds, i.e., whenever $|d_t| > f_r/2N_t$. This “early-onset” Doppler aliasing is a result of the DDMA MIMO processing.

There is one important difference, however, between DDMA Doppler aliasing and the SIMO Doppler aliasing. Specifically, in DDMA, fast target echoes from the n^{th} transmit signal will be received and processed in such a way as to become Doppler ambiguous with slow targets ($d_{t'} \in D^{SLOW} \equiv \{d_{t'} : |d_{t'}| \leq f_r/2N_t\}$) from a different MIMO transmitter. This relationship is made explicit by writing the transmit array response vector as a function of $\Theta_{t'} = \{\theta_{t'}, \zeta_{t'}, d_{t'}, z_{t'}\}$, which includes several additional target parameters such as the target Doppler $d_{t'}$ and target range zone $z_{t'}$. For DDMA, $\mathbf{a}_{Tx}(\theta_t, \zeta_t, d_t \in D^{FAST}, z_t)$ is a permutation of $\mathbf{a}_{Tx}(\theta_{t'}, \zeta_{t'}, d_{t'} \in D^{SLOW}, z_{t'})$. This property results in a unique kind of ambiguity, as illustrated in Figure 3.

The exact way in which elements of the $\mathbf{a}_{Tx}(\theta_t, \zeta_t, d_t \in D^{FAST}, z_t)$ are permuted to form the elements of $\mathbf{a}_{Tx}(\theta_{t'}, \zeta_{t'}, d_{t'} \in D^{SLOW}, z_{t'})$ depends on the order that the DDMA frequencies are mapped to transmitters. The standard linear mapping, (6), results in a cyclic permutation. That is, $\mathbf{a}_{Tx}(\theta_t, \zeta_t, d_t \in D^{FAST}, z_t)$ is formed by circular shifting (or rotating) of $\mathbf{a}_{Tx}(\theta_{t'}, \zeta_{t'}, d_{t'} \in D^{SLOW}, z_{t'})$. The size of this shift, N_{shift} , depends on the size of $d_t \in D^{FAST}$. If $|d_t|$ is large, the shift will be large; if $|d_t|$ is small, the shift will be small. Quantitatively, we may define:

$$N_{shift} = \text{sign}(d_t) \lfloor (|d_t| + f_r/2N_t) / (f_r/N_t) \rfloor \quad (15)$$

and

$$d'_t = d_t - N_{shift} f_r / N_t \quad (16)$$

where $\lfloor \cdot \rfloor$ denotes the floor operation, $\text{sign}(x) = 1$ when $x \geq 0$, and $\text{sign}(x) = -1$ if $x < 0$. Then, $\mathbf{a}_{Tx}(\theta_t, \zeta_t, d_t \in D^{FAST}, z_t)$ is formed by circular shifting N_{shift} times, i.e.,

$$\mathbf{a}_{Tx}(\theta_t, \zeta_t, d'_t, z_t) \xrightarrow{\text{Shift by } N_{shift}} \mathbf{a}_{Tx}(\theta_t, \zeta_t, d_t, z_t). \quad (17)$$

For uniform linear arrays, this permutation causes strong “ambiguities.” For uniform linear arrays, the target response vector when $d'_t \in D^{SLOW}$ takes the form:

$$\mathbf{a}_{Tx}(\Theta_t) = \begin{bmatrix} e^{j\psi_1} & e^{j\psi_2} & \dots & e^{j\psi_{N_t}} \end{bmatrix}^T, \quad \psi_n = (n-1)\psi \quad (18)$$

where $\psi = 2d_E \cos(\zeta_t) \sin(\theta_t) / \lambda$. Note that the elements of (18) have linear phase slope. For fast targets, (18) is circularly shifted N_{shift} times. Nonetheless, the shifted vector still has the same linear phase slope, except for a phase discontinuity at element N_{shift} . Depending on the location of this phase discontinuity, the resulting array response can vary from a “sum” to “difference” pattern when computed over the non-rotated manifold. Regardless of discontinuity location, the resulting response vector is highly correlated with slow-speed targets near the same angle, resulting in a “near” ambiguity. At certain target Dopplers, moreover, this linear phase progression will be nearly the same as that of clutter. As such, clutter nulls can appear ambiguously in Doppler.

3.4. Avoiding Ambiguities with Normal DDMA

Nonuniformly sampled linear (or planar) arrays, of course, do not have response vectors of the form (18). Nonplanar arrays are also unlikely to have response vectors of the form of (18). Consequently, such array topologies provide one approach toward mitigating the Doppler ambiguity problem described in Section 3.3.

Unfortunately, most radars use uniform linear (or uniform planar) array topologies. Such topologies dominate the marketplace due low manufacturing costs and many other practical reasons. Hence, other approaches toward mitigating the Doppler ambiguity problem are needed. Such techniques are the focus of the next section.

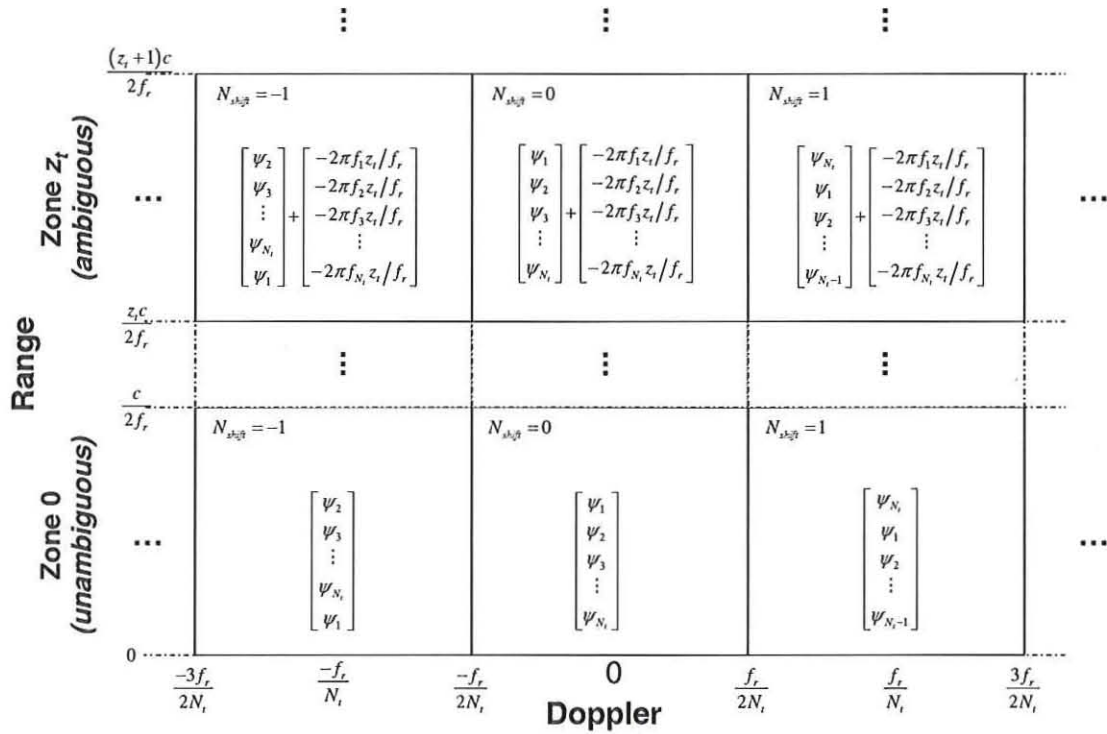


Figure 3. Transmitter-dependent phase values in $\mathbf{a}_{Tx}(\Theta_t)$ for linearly mapped DDMA waveform (6).

4.0 Dithered DDMA

To eliminate the DDMA blind speeds described in Section 3.3, we developed two modified DDMA techniques. Collectively, we call these “dithered DDMA” techniques. The first technique works by altering the mapping between DDMA transmit frequencies and transmit antennas. The second technique, in contrast, adds a phase offset to each of the transmitted waveforms. In both cases, these techniques work by altering the array response vectors for fast targets, thereby suppressing ambiguities. Better still, these techniques are complementary, meaning they can be used together for even greater benefit.

4.1. Frequency-Dithered DDMA

In a frequency-dithered DDMA system, we alter the mapping of DDMA frequencies to transmit antennas. This, in turn, modifies the permutation so that it can no longer be represented as a series of circular shifts, i.e.:

$$\mathbf{a}_{Tx}(\theta_t, \zeta_t, d'_t, z_t) \xrightarrow{\text{Permutation} \neq \text{Shift by } N_{\text{shift}}} \mathbf{a}_{Tx}(\theta_t, \zeta_t, d_t, z_t). \quad (19)$$

The goal is to choose a mapping that alters $\mathbf{a}_{Tx}(\Theta_i)$ in some favorable way. The mapping could, for example, be pseudo-random (which provides good performance over all angles). The mapping could also be optimized to favor specific target angles and speeds.**

The impact of pseudo-random frequency-dithering is clearly illustrated in Figure 4. Here, we plot the SINR loss for an airborne GMTI radar having the same parameters as in . Away from the broadside region (i.e., toward the left or right sides of Figure 4a), the impact of frequency-dithering is particularly evident. In these regions, the array response vector's phase slope, $\psi = 2d_E \cos(\zeta_i) \sin(\theta_i) / \lambda$, will be large because $|\psi| \gg 0$. Random permutations of $\mathbf{a}_{Tx}(\theta_i, \zeta_i, d'_i \in D^{SLOW}, z_i)$ thus result in response vectors, $\mathbf{a}_{Tx}(\theta_i, \zeta_i, d_i \in D^{FAST}, z_i)$, that generally have a small projection onto their unpermuted counterparts, $\mathbf{a}_{Tx}(\theta_i, \zeta_i, d'_i \in D^{SLOW}, z_i)$. Consequently, this allows good nulling of clutter at the same angle as the fast target.

Near the broadside region, however, $\mathbf{a}_{Tx}(\theta_i, \zeta_i, d'_i \in D^{SLOW}, z_i)$ has a small phase slope $|\psi|$. Consequently, random permutations of $\mathbf{a}_{Tx}(\theta_i, \zeta_i, d'_i \in D^{SLOW}, z_i)$ will result in response vectors, $\mathbf{a}_{Tx}(\theta_i, \zeta_i, d_i \in D^{FAST}, z_i)$, that are much closer to their unpermuted counterparts. In the extreme (i.e., at array broadside, where $\mathbf{a}_{Tx}(\theta_i, \zeta_i, d'_i \in D^{SLOW}, z_i) = [1 \ \dots \ 1]^T$ and $\psi = 0$), this distance becomes zero; hence, permuting $\mathbf{a}_{Tx}(\theta_i, \zeta_i, d'_i \in D^{SLOW}, z_i)$ has no effect on it. Therefore, it can be difficult (or impossible) to detect fast targets near-broadside region. This point is illustrated in Figure 4b, which shows the SINR loss at broadside. Note that N_t blind speeds are present, despite frequency-dithering. Another technique must be used to suppress blind speeds in the broadside region.

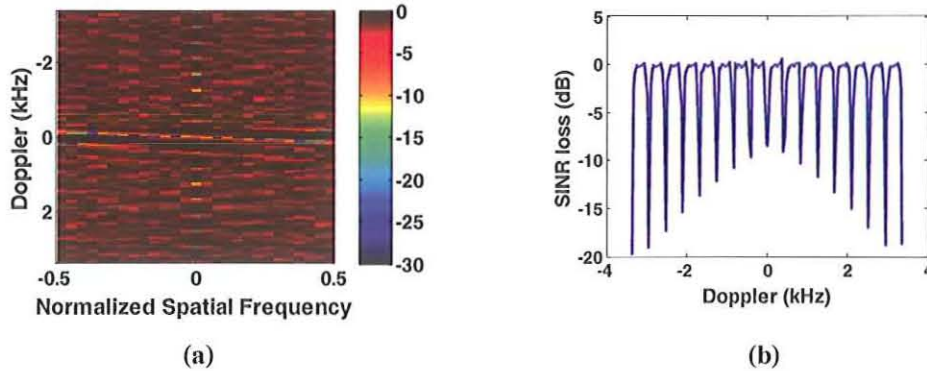


Figure 4. GMTI radar using Frequency-Dithered DDMA waveform.
(a) SINR Loss, (b) SINR loss at broadside

** For example, the mapping $\{f_1, f_N, f_2, f_{N-1}, \dots\} \rightarrow \{Tx1, Tx2, Tx3, Tx4, \dots\}$ shifts targets in Doppler zone 2 so that they compete with clutter from angle $-\theta$. This sort of mapping might be used when the transmit antenna has low gain toward $-\theta$ (because targets in Doppler zone 2 will compete with clutter that is weak and unlikely to cause a blind speed). There are many other similar specialized mappings that might be considered.

4.2. Phase-Dithered DDMA

Near the broadside region, frequency-dithered DDMA fails to mitigate the DDMA blind speeds discussed in Section 3.3. Fortunately, a second technique, called “phase-dithered DDMA,” works well in this region.

In a phase-dithered DDMA system, we add a phase offset to each of the DDMA transmit signals. That is, we transmit

$$s_n(t) = s(t)e^{jv_n(p)+jv_n}. \quad (20)$$

Note that the n^{th} transmitter has been assigned a phase value v_n .

On receive, the MIMO processor applies matched filters for both the frequency and the phase of the transmitted signal. For $d_t \in D^{\text{SLOW}}$, this process removes the transmit phase v_n (i.e., it multiplies the received signal by e^{-jv_n}). For $d_t \in D^{\text{FAST}}$, however, the target signal will appear at the output of the “wrong” matched filter (e.g., it appears in matched filter $n + N_{\text{shift}}$, assuming a linear DDMA mapping is used as in (6)) due to the Doppler ambiguity effect. As discussed in Sections 4.0 and 4.1, this will cause the target to have a permuted transmit array response vector. Likewise, it will have the “wrong” set of phases removed (i.e., it will be multiplied by $e^{-jv_{n+N_{\text{shift}}}}$, resulting in a phase residue of $v_n - v_{n+N_{\text{shift}}}$). Choosing v_n to be uniformly random on $[0, 2\pi]$ makes these phase residuals random, providing robust performance over all angles. Other choices of v_n can be used to optimize performance over smaller angular sectors.

Interestingly, this idea of inserting a spatially varying phase dither and then later removing it, with the net effect of shifting undesired signals away from the desired signal subspace, is not new. This same idea has been used, previously, to mitigate nonlinear distortion effects originating in the radar electronics [20]. For this work, we merely adapted the concept to MIMO radar.

Figure 5 illustrates the impact of phase-dithering applied to DDMA. Here, the N_t phase values, $\{v_n\}$, were taken to be uniformly random on $[0, 2\pi]$. Pseudo-random frequency-dithering was also used. Note that the losses due to ambiguous clutter near broadside (Figure 5b) have been replaced with a much smaller loss spread over the entire Doppler space.

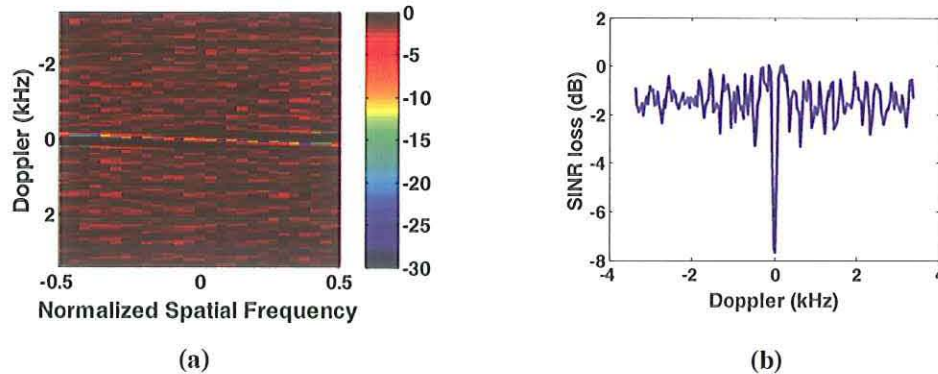


Figure 5. GMTI radar using Phase-Dithered DDMA waveform.
(a) SINR Loss, (b) SINR loss at broadside

4.3. Range Ambiguities

In pulse-Doppler radar, range ambiguities occur whenever there are detectable echoes from targets (or clutter) at ranges greater than $c/2f_r$. Ranges under $c/2f_r$ are said to be unambiguous, whereas ranges $z_i c/2f_r < \rho_i \leq (z_i + 1)c/2f_r$ are said to lie in the z_i -th ambiguous range zone.

In DDMA MIMO radar, range ambiguous response vectors $\mathbf{a}_{Tx}(\theta_i, \zeta_i, d_i, z_i)$ will differ from unambiguous responses $\mathbf{a}_{Tx}(\theta_i, \zeta_i, d_i, 0)$, even if both are at the same angle and Doppler. To detect range ambiguous targets, then, the correct steering vector should be used.

For linearly mapped DDMA (as in (6)), the n^{th} element of $\mathbf{a}_{Tx}(\theta_i, \zeta_i, d_i, z_i)$ is shifted by $e^{-j2\pi z_i f_n / f_r}$ as illustrated in Figure 3. This shift has an interesting effect on the response vector $\mathbf{a}_{Tx}(\theta_i, \zeta_i, d_i, z_i)$. In particular, it modulates $\mathbf{a}_{Tx}(\theta_i, \zeta_i, d_i, z_i)$, causing its pattern to point toward a shifted angle. This results in an ambiguity between targets (or clutter) in zone z_i and targets (or clutter) in zone 0 at some shifted angle. The size of this angular shift increases with z_i , meaning that range zones that are “close” will have small angular shifts, while range zones that are far apart have a large angular shifts. This could be an issue; we are often interested in signals received from a small number of range zones that are relatively close together. In such cases, the small angular shifts of the response pattern could result in clutter (or targets) from nearby angles competing with the signal of interest

Frequency dithered DDMA, however, solves this problem. By altering the mapping of frequencies to transmitters, we modify the modulation applied to range-ambiguous response vectors. With certain frequency dithers, for example, we can increase the size of the angular shift applied to nearby range zones^{††}. This type of dithering might be used to better separate signals and clutter in nearby range ambiguities.

Likewise, we could pseudo-randomly map frequencies to transmitters. This type of dithering results in modulation sequences that do not *shift* the angle response. Instead, they impart unique phase signatures onto each range zone’s response vectors. The response vectors from different range regions will thus have low cross-correlation. Furthermore, these response vectors can be used as steering vectors by and adaptive clutter cancellation algorithm (like STAP) – further suppressing range ambiguities (much like the way Doppler ambiguities were suppressed in Section 4.1).

5.0 Summary and Conclusions

In this paper, we examined one promising type of FDMA waveform, in which disjoint Doppler frequency bands were used to isolate the transmitted signals. In particular, these “Doppler Division Multiple Access” waveforms were shown to support high MCR levels. However, these waveforms also suffered from clutter ambiguities and blind speeds. The source of these ambiguities was investigated. Their origin was shown to be the use of linear frequency shifts across a uniform linear antenna aperture.

To address this problem, we proposed a modified DDMA waveform approach. In part, this approach leveraged prior work relating to mitigation of array distortion effects. In simulations, this modified DDMA approach was able to eliminate blind speeds and/or shift them to regions of the Doppler space where they are more tolerable.

REFERENCES

^{††} For example, $\{f_1, f_{N/2+2}, f_3, f_{N/2+4}, f_5, \dots\} \rightarrow \{Tx1, Tx2, Tx3, Tx4, \dots\}$ makes the shift very large. If used in combination with a narrow transmit element pattern, the ambiguous angles may correspond to clutter-free (and target free) regions, which will improve receiver performance.

[1] D.J. Rabideau, P. Parker, "Ubiquitous MIMO multifunction digital array radar," *Proc. Asilomar Conf. Signals, Syst., Comput.*, vol. 1, pp. 1057-64, 2003 (see also extended version DTIC report ADA421233).

[2] D.W. Bliss, K.W. Forsythe, "Multiple-input multiple-output (MIMO) radar and imaging: degrees of freedom and resolution," *Proc. Asilomar Conf. Signals, Syst., Comput.*, vol. 1, pp. 54-9, 2003.

[3] F.C. Robey, S. Coutts, et al., "MIMO radar theory and experimental results," *Proc. Asilomar Conf. Signals, Syst., Comput.*, vol. 1, pp. 300-4, 2004.

[4] I. Bekkerman, J. Tabrikian, "Target Detection and Localization Using MIMO Radars and Sonars," *IEEE Trans Sig Proc*, vol. 54, pp. 3873-83, 2006.

[5] J. Tabrikian, "Barankin Bounds for Target Localization by MIMO Radars," *Proc. IEEE Wksh. Sensor Array & Multichannel Sig. Proc.*, pp. 278-81, 2006.

[6] K.W. Forsythe, D.W. Bliss, "Waveform Correlation and Optimization Issues for MIMO Radar," *Proc. Asilomar Conf. Signals, Syst., Comput.*, pp. 1306-10, 2005.

[7] K.W. Forsythe, D.W. Bliss, et al., "Multiple-input multiple-output (MIMO) radar: performance issues," *Proc. Asilomar Conf. Signals, Syst., Comput.*, vol. 1, pp. 310-5, 2004.

[8] J. Li, P. Stoica, "MIMO Radar with Colocated Antennas," *Signal Processing Magazine, IEEE*, vol. 24, pp. 106-14, 2007.

[9] A.M. Haimovich, R.S. Blum, et al., "MIMO Radar with Widely Separated Antennas," *Signal Processing Magazine, IEEE*, vol. 25, pp. 116-29, 2008.

[10] G.J. Frazer, Y.I. Abramovich, et al., "Multiple-input multiple-output over-the-horizon radar: experimental results," *Radar, Sonar & Navigation, IET*, vol. 3, pp. 290-303, 2009.

[11] C.-Y. Chen, P.P. Vaidyanathan, "MIMO Radar Space-Time Adaptive Processing Using Prolate Spheroidal Wave Functions," *Signal Processing, IEEE Transactions on*, vol. 56, pp. 623-35, 2008.

[12] B. Friedlander, "Waveform Design for MIMO Radars," *IEEE Trans AES*, vol. 43, pp. 1227-38, 2007.

[13] J. Bergin, S. McNeil, et al., "MIMO Phased-Array for SMTI Radar," *Proc. 2008 IEEE Aerospace Conf.*, pp. 1-7, 2008.

[14] D. Hai, "Polyphase code design for Orthogonal Netted Radar systems," *IEEE Trans Sig Proc*, vol. 52, pp. 3126-35, 2004.

[15] H.A. Khan, D.J. Edwards, "Doppler problems in orthogonal MIMO radars," *Proc. IEEE Radar Conf.*, pp. 244-7, 2006.

[16] B. Liu, Z. He, et al., "Polyphase Orthogonal Code Design for MIMO Radar Systems," *Proc. CIE Int. Conf. on Radar*, pp. 1-4, 2006.

[17] E. Fishler, A. Haimovich, et al., "Spatial diversity in radars-models and detection performance," *IEEE Trans Sig Proc*, vol. 54, pp. 847-57, 2006.

[18] D.J. Rabideau, "MIMO radar with widely separated antennas," *IEEE Trans AES*, vol. 43, pp. 1227-38, 2007.

[19] J. Ward, "Space-Time Adaptive Processing for Radar," *IEEE Trans AES*, vol. 39, pp. 917-30, 1991. Tech. Rpt. TR-1015, 13 Dec. 1994.

[20] L.C. Howard, N.K. Simon, et al., "MIMO Radar with Widely Separated Antennas," *IEEE Trans Sig Proc*, vol. 56, pp. 127-38, 2008. Independent phase diversity, *IEEE Trans Sig Proc*, vol. 56, pp. 1525-8, 2008.

stut A

1110
- Barbara Martin
voice mail

12/10 -
Archives
confirmed that
TR-1015 is
stut A.

IEEE Trans
Laboratory,
igital phased
IEEE MTT-S